Journal of Magnetic Resonance **143,** 299–310 (2000)
doi:10.1006/jmre.1999.1991, available online at http://www.idealibrary.com on IDEAL®

Broadband Echo Sequence Using a π Composite Pulse for the Pure NQR of a Spin $I = \frac{3}{2}$ Powder Sample

Christophe Odin

Groupe Matière Condensée et Matériaux (GMCM–UMR 6626), Université Rennes I, Campus de Beaulieu, 35042 Rennes Cedex, France

E-mail: christophe.odin@univ-rennes1.fr

Received July 9, 1999; revised September 30, 1999

This work presents a numerical approach to optimizing sequences with composite pulses for the pure NQR of a spin $I = \frac{3}{2}$ powder sample. The calculations are based on a formalism developed in a previous paper, which allows a fast powder-averaging procedure to be implemented. The framework of the Cayley–Klein matrices to describe space rotations by 2 × 2 unitary and unimodular complex matrices is used to calculate the pulse propagators. The object of such a study is to design a high-performance echo sequence composed of a single preparation pulse and a three-pulse composite transfer pulse. We mean a sequence leading to a large excitation bandwidth with a good signal-to-noise ratio, a flat excitation profile near the irradiation frequency, and a good linearity of the phase as a function of frequency offset. Such a composite echo sequence is intended to give a better excitation profile than the classical Hahn (θ)–τ–(2θ) echo sequence. It is argued that in pure NQR of a powder sample, the sequence must be optimized *as a whole* **since both the excitation and the reception of the signal depend on the relative orientation of the crystallites with respect to the coil axis. To our knowledge, this is the first time such a global approach is presented. An extensive numerical study of the composite echo sequence described above is performed in this article. The key of the discrimination between the sequences lies in using the first five reduced moments of the excitation profile as well as an estimator of the phase linearity. Based on such information, we suggest that the echo sequence that best fulfills our criterion is $(1)_0$–τ–$(0.35)_0(2.1)_\pi(0.35)_0$, the pulse angles $\omega_{RF}t_p$ being in radians. The subscripts are the relative pulse phases. We outlined the way to implement the spin echo mapping method to reconstruct large spectra with this sequence, and it is shown that it reduces the acquisition time by a factor of 1.7 if compared to the classical Hahn echo. Some other broadband echo sequences are also briefly discussed. We also study the effect of a small delay between the pulses of the composite pulse to take into account the experimental constraint imposed by the spectrometer. To be complete, we give an estimation of the performances of the Hahn echo, the stimulated echo, and the composite echo sequence optimized for a powder sample when applied to a monocrystal. Experiments performed on chloranil at ambient temperature confirm the predicted excitation profiles.**

Key Words: **NQR; composite pulses; excitation bandwidth; powder average.**

I. INTRODUCTION

More and more domains in physics are busy with samples presenting a broad distribution of quadrupolar interactions (glasses, incommensurate structures, high-temperature superconductors, alloys, etc.), which make necessary the acquisition of large spectra. In this article, we are mainly interested in designing an echo pulse sequence which allows a broad and flat excitation profile near the irradiation frequency, with good phase linearity as a function of the frequency offset, in order to acquire large spectra for the pure NQR of spin $I = \frac{3}{2}$ powder samples. We propose an echo sequence using a three-pulse composite transfer pulse, which reduces the reconstruction time of large spectra by a factor of 1.7 if compared to the use of a classical Hahn echo sequence.

A composite pulse is a sequence of pulses ideally placed side by side and combined in a way to give the same result as an equivalent single pulse of given length and phase. These composite pulses are supposed to compensate the "imperfections" occurring with single pulses, such as radiofrequency spatial inhomogeneities and finite bandwidth excitation (*1*). In general, the compensation of all existing imperfections could not be achieved simultaneously and, obviously, only the final result the experimenter wants to obtain decides which imperfection is the most important to be compensated. Usually, the designer of composite pulses has to find a compromise between sensitivity, excitation bandwidth, linearity of the phase with respect to the frequency offset, and an excitation profile as flat as possible around the excitation frequency to minimize the deformation of the spectrum. Broadband excitation by composite pulses have been the subject of lots of studies, mainly in NMR (*1–5*), but to our knowledge, only a few applications concerned NQR (*6–9*).

We have a double reason for presenting a new analysis of composite pulses in NQR. First, most composite sequences were designed to optimize the conversion efficiency of so-called "$\pi/2$" or "π" pulses. But the π pulses were usually optimized to create a population inversion $I_z \Rightarrow -I_z$. Such pulses can be used, for instance, for T_1 inversion-recovery

1090-7807/00 $35.00

measurements. However, such optimized π composite pulses are not suitable for an echo sequence, because the second π pulse must transform a coherence of order $p = +1$ into $p = -1$: $I_+ \Rightarrow I_-$. The second reason is more fundamental. Although NMR composite sequences may also be efficient for some experiments in pure NQR of a single crystal (at least for a spin $I = \frac{3}{2}$), the analysis leading to their form is *not* valid for a powder sample in NQR. Simply because in pure NQR of a powder sample, the nutation angles and the reception amplitude have an intrinsic angular dependence, even with an ideal coil giving no spatial radiofrequency inhomogeneities. More precisely, the nutation angle and reception amplitude are modulated by a function depending on the polar angles of the coil axis with respect to the principal axis of the electric field gradient at the nucleus. This angular dependence is related to the irradiation frequency mismatch. As both "imperfections" operate together, they must be treated simultaneously. Therefore, even with an ideal experimental setup, one has to deal with an inherent distribution of excitation/reception sensitivity, which averages the signal. As a consequence of this powder average, the sequence must be optimized *as a whole.* One cannot use the simpleminded approach of building new sequences by combining already optimized composite pulses because the powder average needs to be done over the whole sequence. A similar analysis is also valid for the NMR of powder samples when the pulses cannot be considered "hard" anymore, because an orientation-dependent term appears in the pulse propagator.

To our knowledge, such a global analysis of an echo sequence has not been performed yet, and the object of this article is to propose a numerical approach in the case of a "Hahn" echo sequence for pure NQR of spin $I = \frac{3}{2}$.

Since the aim of this work is to achieve the acquisition of a large spectrum in a single run, our criteria will favor the flatness of the excitation profile near the irradiation frequency and the linearity of the phase as a function of the frequency offset. Obviously, the price to be paid for these advantages is a loss of sensitivity. The calculation of the composite pulse response can be performed with the Magnus expansion techniques (*4*). On the one hand, such techniques are appealing because they give analytical results which lead to a better insight into the way to design broadband composite pulse sequences. But on the other hand, these techniques usually become useless at large frequency offsets because the perturbation approach breaks down. It is also clear that the powder average cannot be performed analytically in general, thus losing most of the interest of having explicit expressions. For these reasons, we decided to concentrate our efforts on a numerical approach.

Almost infinite possibilities of pulse combinations are allowed to obtain an equivalent composite π pulse. It was shown in NMR that long composite pulses lead to a better compensation of the imperfections. However, because composite pulses are much longer than usual single pulses, these possibilities are mainly limited by the equilibration time of the spin system under the RF irradiation (the so-called $T_{2\rho}$ time) and by experimental problems such as coil arcing and heating and power drop off. Therefore, only "short" (as compared to the timescales of the phenomena discussed above) composite pulses are usually experimentally accessible. Thus, we limited our investigations to an echo sequence with a single preparation pulse and a transfer composite π pulse composed of three pulses. We will neglect all the experimental imperfections that would not exist if one were using an ideal spectrometer of finite power, a perfect coil and resonant circuit, etc.

This article is divided as follows. After a brief presentation of the analogy between the theory of pure NQR of spin $I = \frac{3}{2}$ and high-field NMR of an isolated spin, we calculate the time evolution of the density operator using the formalism of Cayley–Klein matrices to handle the product of three-dimensional rotations (Section II). Then, we present the main results of a brute force computer simulation which optimizes the composite echo sequence built with a single preparation pulse and a transfer composite π pulse composed of three separated pulses (Section III). The performances of the most efficient composite echo sequences are compared to those obtained with a two-pulse Hahn echo sequence and a three-pulse stimulated echo sequence. The simulated excitation profiles are validated by experimental data coming from experiments performed on chloranil at ambient temperature (Section IV). An estimation of the performance of the sequences optimized for powder samples is also given when they are applied to a monocrystal (Section V). The last section (Section VI) is devoted to an implementation of the spin echo mapping procedure to reconstruct large spectra (*10*) with the optimized composite echo sequence derived in Section III.

II. THEORY

This section is devoted to a brief account of the general features of a formalism developed in a previous article (*11*) to handle pure NQR of spin $I = \frac{3}{2}$, and to present the Cayley–Klein formalism used in the computer simulations. Other formalisms can be found in (*12–15*). The theory is then applied to the classical Hahn echo sequence (HES) (θ)–τ–(2θ) (Fig. 1a), to the stimulated echo sequence (SES) (θ)–τ–(θ)–τ'–(θ) (Fig. 1b), and to the composite echo sequence (CES) composed of a preparation pulse of fixed angle, a mixing delay τ, and a refocusing composite π pulse (CPP) composed itself of three different pulses side by side or separated by a short free evolution period of known duration (θ_0)–τ–$(\theta_1)(\theta_2)(\theta_3)$ (Fig. 1c).

The Cartesian representation of the pure quadrupolar part of the Hamiltonian of a spin $I = \frac{3}{2}$ nucleus of quadrupole moment M_Q is

$$H_q = \frac{1}{6}\frac{eM_QV_{zz}}{2}\left\{3I_z^2 - \frac{15}{4} + \frac{\eta}{2}(I_+^2 + I_-^2)\right\}, \qquad [1]$$

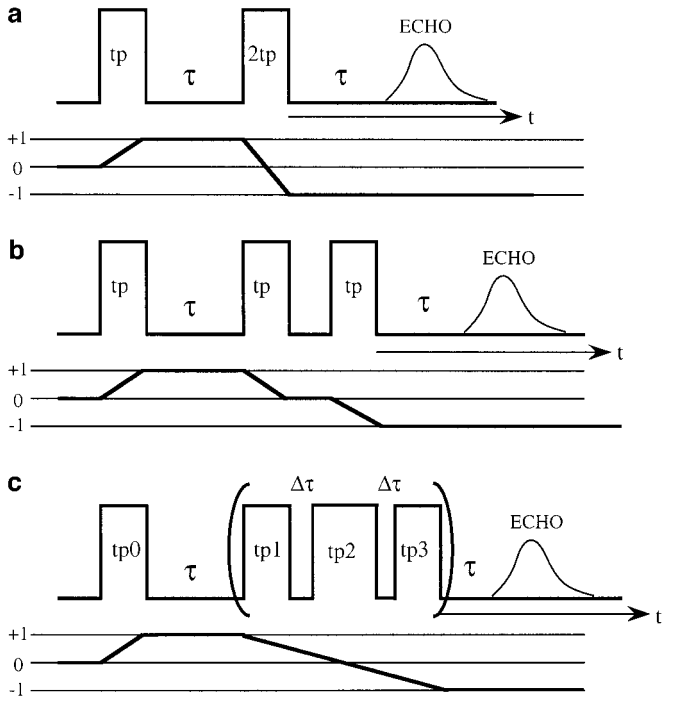

FIG. 1. Pulse sequences with their coherence pathways. (a) Classical Hahn echo sequence (HES); (b) stimulated echo sequence (SES); (c) composite echo sequence (CSE) with a transfer pulse composed of three pulses. In the ideal sequence, the delay $\Delta\tau$ between the pulses is zero. For a real sequence, this delay is imposed by the spectrometer electronics.

where

$$\eta = \frac{V_{xx} - V_{yy}}{V_{zz}} \qquad [2]$$

is the asymmetry parameter. $0 \leq \eta \leq 1$ if $|V_{xx}| \leq |V_{yy}| \leq |V_{zz}|$. The Cartesian spin operators $\{I_x, I_y, I_z\}$ are quantified in the principal axis system (PAS) of the electric field gradient (EFG) tensor $V_{\alpha\beta} = (\partial^2 V/\partial\alpha\partial\beta)$ at the nucleus under study, the z axis being oriented along the direction of the highest eigenvalue in absolute value. In the following, the Hamiltonians are expressed in units of angular frequencies ($\hbar = 1$). We neglect all other contributions to the Hamiltonian, such as dipolar interactions or a residual Zeeman interaction.

When a linearly polarized radiofrequency field (RF) of phase φ irradiates the sample, one has to add the RF Hamiltonian H_{RF} to the quadrupolar Hamiltonian,

$$H_{\mathrm{RF}} = 2\omega_{\mathrm{RF}}\cos(\omega t + \varphi)\mathbf{I}\cdot\mathbf{n}, \qquad [3]$$

where $\omega_{\mathrm{RF}} = \gamma B_1/2$, γ is the magnitude of the nuclear gyromagnetic ratio, and ω is the excitation angular frequency. Vectors are noted in bold letters: $\mathbf{I} = I_x\mathbf{i} + I_y\mathbf{j} + I_z\mathbf{k}$, where $\mathbf{i}$, $\mathbf{j}$, $\mathbf{k}$ are the unit vectors of the PAS. The coil axis is directed along the unit vector $\mathbf{n}$ whose coordinates are $\{\sin(\theta)\cos(\phi), \sin(\theta)\sin(\phi), \cos(\theta)\}$ in the PAS of the EFG.

It was shown elsewhere (*11*) that the operator formalism to handle pure NQR of spin $I = \frac{3}{2}$ could be reduced to the same formalism used in the case of the high-field NMR of an isolated single spin subjected to an off-resonance RF irradiation. Within this framework, the secular part of the NQR Hamiltonian during a pulse is in the "rotating frame"

$$H = \Delta\omega Q_z + 2\lambda\omega_{\mathrm{RF}}\{\cos(\zeta)Q_x + \sin(\zeta)Q_y\}, \qquad [4]$$

where the pulse phase is $\varphi = \zeta - \frac{\pi}{2}$.

The angular factor $\lambda = \lambda(\theta, \phi)$ is a function of the polar angles which specify the orientation of the coil with respect to the PAS of the EFG

$$\lambda(\theta, \phi) = \frac{1}{2a\sqrt{3}} \times \sqrt{4\eta^2\cos^2(\theta) + \sin^2(\theta)[9 + \eta^2 + 6\eta\cos(2\phi)]}, \qquad [5]$$

where $a = \sqrt{1 + \eta^2/3}$.

The normalized operators Q_α fulfill the same commutation relations as the Cartesian spin operators

$$[Q_x, Q_y] = iQ_z \text{ and cyclic permutations} \qquad [6]$$

$$\mathrm{Tr}[Q_\alpha Q_\beta] = \delta_{\alpha\beta} \quad \text{for } \alpha = x, y, z. \qquad [7]$$

Therefore, usual transformation rules (*16–18*) can be applied to calculate the time evolution of the density operator, because the Hamiltonian H is time independent.

In the high-temperature approximation, the initial condition can be taken as

$$\rho(0) = Q_z \sim \rho_{\mathrm{eq}}, \qquad [8]$$

where ρ is the density operator in the rotating frame. All calculations can then be performed by developing the density operator on the Liouville space spanned by the basis $\{Q_+, Q_-, Q_z\}$: $\rho(t) = r_+(t)Q_+ + r_z(t)Q_z + r_-(t)Q_-$, the different factors being calculated by following the coherence pathways. This shows that the time evolution of the density operator is similar to combining three-dimensional rotations. A simple and fast method for evaluating the amplitude associated with the coherence pathways is given below.

When a single site of given orientation with respect to the coil is considered, a quadrature detection setup will give the signal

$$S(t, \lambda) = 2\lambda\mathrm{Tr}\{Q_+\rho(t)\}, \qquad [9]$$

with $\rho(t)$ the density operator at time t in the rotating frame.

The powder average of signal $S(t, \lambda)$ is then

$$S(t) = \langle S(t, \lambda) \rangle = \int_{\lambda_{min}}^{\lambda_{max}} g(\lambda) S(t, \lambda) d\lambda, \qquad [10]$$

where $g(\lambda)$ is the probability density of variable λ. The probability density $g(\lambda)$ depends on the asymmetry parameter η, and was calculated analytically in (*11*). To be complete, the analytical expression of $g(\lambda)$ is given in the Appendix. Evidently, the powder average can also be performed in the usual way by considering that all angles (θ, ϕ) are distributed randomly, but the calculations are much slower than the suggested method.

A way of calculating the combination of rotations is the formalism of the Cayley–Klein (CK) matrices (*19–22*). Instead of using real 3×3 matrices belonging to group SO(3), rotations through an arbitrary set of Eulerian angles are represented by 2×2 unitary complex matrices with determinant unity (group SU(2)). Such a formalism can be applied to calculate the time evolution of the density operator.

Let us define a matrix of operators X and a matrix of complex numbers U as

$$X = \begin{pmatrix} Q_z & Q_x + iQ_y \\ Q_x - iQ_y & -Q_z \end{pmatrix} = \begin{pmatrix} Q_z & Q_+ \\ Q_- & -Q_z \end{pmatrix} \qquad [11]$$

$$U = \begin{pmatrix} A & B \\ -B^* & A^* \end{pmatrix} \quad \text{and} \quad AA^* + BB^* = 1, \qquad [12]$$

where the * denotes the complex conjugate and the + the hermitic conjugate.

The CK matrix U is the propagator of a pulse sequence $P_1 P_2 \ldots P_m$, where P_i represents either a pulse or a free evolution period. U is the product of the corresponding CK matrices $U = U_1 U_2 \ldots U_m$ *in the same order*, to allow the right pulse phase propagation. Such matrices will be described below.

Note that the product of two CK matrices $U_1 U_2$ is again a CK matrix U with parameters

$$\begin{cases} A = A_1 A_2 - B_1 B_2^* \\ B = A_1 B_2 + B_1 A_2^* \end{cases}. \qquad [13]$$

Then, straightforward iterative procedures permit the calculation of every general product of CK matrices.

After a pulse sequence of resulting CK matrix U, matrix X representing the set of operators $\{Q_+, Q_-, Q_z\}$ is transformed into the matrix of operators X' as

$$X' = UXU^+ = \begin{pmatrix} \alpha & \beta \\ \beta^+ & -\alpha \end{pmatrix} \qquad [14]$$

with

$$\begin{cases} \alpha = AB^* Q_+ + A^* B Q_- + (AA^* - BB^*) Q_z \\ \beta = A^2 Q_+ - B^2 Q_- - 2AB Q_z \end{cases}. \qquad [15]$$

The interpretation of this transformation is straightforward: the pulse sequence described by CK matrix U transforms initial operator Q_z into operator α and initial operator Q_+ into β. The amplitudes associated with the coherence transfers are directly given by the factors in front of the operators $\{Q_+, Q_-, Q_z\}$. For instance, starting with the initial zero-quantum coherence $p = 0$, the amplitudes associated with coherence transfers $\Delta p = 0, -1, 1$ are respectively $(AA^* - BB^*)$, A^*B, and AB^*.

In other words, how a pulse sequence of resulting CK matrix U transforms the initial equilibrium state $\rho(0) = Q_z$ is simply a matter of calculating products of 2×2 matrices. However, it is faster to calculate the matrices corresponding to some groups of pulses (a single pulse, a free evolution period, a single pulse followed by a free evolution period, a composite pulse, etc.), and to combine the resulting amplitudes by following the coherence pathway(s).

Concerning the pure spin $I = \frac{3}{2}$ NQR, the propagator of a single pulse of duration t_p and phase φ is written as

$$U = \begin{pmatrix} a & -ibe^{i\varphi} \\ ibe^{-i\varphi} & a^* \end{pmatrix} \qquad [16]$$

with

$$\begin{cases} a = \cos(v/2) - i \sin(v/2)\sin(u) \\ b = \cos(u)\sin(v/2) \end{cases}. \qquad [17]$$

Note that the phase of the pulse is present only on the diagonal of matrix U and that b is a real number. The other parameters are

$$\begin{cases} \cos(u) = \dfrac{2\lambda\omega_{RF}}{\omega_e} \\ \sin(u) = \dfrac{\omega}{\omega_e} \end{cases}, \qquad [18]$$

where

$$\begin{cases} \omega_e^2 = \omega^2 + 4\lambda^2\omega_{RF}^2 \\ v = \omega_e t_p = \theta\sqrt{x^2 + 4\lambda^2} \\ x = \dfrac{\omega}{\omega_{RF}} \end{cases}. \qquad [19]$$

v is the effective nutation angle of the pulse, and x is the reduced frequency offset. Below, the expression "pulse angle" will refer to $\theta = \omega_{RF} t_p$. As a rule of thumb, the angle that

maximizes the response to a single pulse in a powder sample is $\theta_M \approx 1$ rad.

The case of free evolution is particularly simple since

$$\begin{cases} a = e^{-i\Delta\omega t/2} \\ b = 0 \end{cases}. \quad [20]$$

Let us calculate the echo amplitude after the usual HES. It uses coherence pathway $0 \rightarrow +1 \rightarrow -1$, that is, transfers of coherence of order $\Delta p = +1$ and -2. The resulting echo amplitude is then

$$\text{HES or CES echo amplitude} \sim \langle \lambda a_0 b_0 B^2 \rangle \quad [21]$$

with a_0 and b_0 the CK parameters of the first pulse and B the CK parameter of the matrix representing either a single or a composite refocusing π pulse. B is calculated from the product of three CK matrices for an ideal composite pulse or from the product of five CK matrices when a free evolution period is inserted in between the pulses.

Concerning the SES echo amplitude, we obtained from the transfers of coherence of order $\Delta p = +1, -1$, and -1

$$\text{SES echo amplitude} \sim \langle \lambda a_0 b_0 (-2 a_0 b_0) a_0^* b_0 \rangle. \quad [22]$$

All pulses have the same duration.

III. COMPUTER SIMULATIONS

This section introduces the main ingredients we used to carry out the numerical optimization of a serie of (CES).

First of all, we chose some criterion to characterize the pulse sequence excitation profile. Since we are interested in a large and flat excitation profile, as well as good phase linearity, a possible key of the discrimination between the sequences lies in using the first five reduced moments of the excitation profile as well as an estimator of the phase linearity.

We denote the complex excitation profile *after powder average* by

$$S_c(x) = M(x) e^{iS(x)}. \quad [23]$$

$M(x)$ is the excitation profile and $S(x)$ is the phase distortion as a function of the reduced frequency offset

$$x = \frac{\omega}{\omega_{RF}}.$$

The product $M(x)dx$ can be interpreted as the probability of exciting the ensemble of nucleus whose reduced frequencies lie in the range $[x, x + dx]$. Thus, it turns out that the simplest simpleminded way to discriminate between the different sequences is to characterize the excitation profile $M(x)$ by its different moments to reduce the amount of information to handle. The centered moments of the excitation profile $M(x)$ are defined as

$$M_0 = \int M(x)dx \quad [24]$$

$$\mu_1 = \frac{\int x M(x) dx}{M_0} \quad [25]$$

$$\mu_n = \frac{\int (x - \mu_1)^n M(x) dx}{M_0} \quad \text{for } n \geq 2. \quad [26]$$

We also need the reduced third and fourth moments:

$$r_3 = \frac{\mu_3}{(\mu_2)^{3/2}} \quad [27]$$

$$r_4 = \frac{\mu_4}{(\mu_2)^2} - \frac{(\mu_3)^2}{(\mu_2)^3} - 1. \quad [28]$$

M_0 is the integrated intensity of the signal over the observed frequency range. μ_1 is the center of gravity: a departure from zero shows that the excitation is not maximum at the irradiation frequency. The square root of the second moment μ_2 gives an estimation of the width of the excitation band (it is obviously the standard deviation of the excitation profile). The reduced third moment r_3 measures the skewness of the excitation profile. A large negative value of r_3 would correspond to a long tail in the excitation profile below the center of gravity and a more compressed profile above the center of gravity.

The reduced fourth moment r_4 gives a rough criterion for discriminating between a *unimodal* or a *bimodal* form of the excitation profile. If $r_4 > 1$, then we have an unimodal behavior, whereas if $r_4 < 1$ the behavior is bimodal. Notice that for a pure Gaussian profile, $\mu_4 = 3(\mu_2)^2$ and $r_4 = 2$. As an example, let us consider a profile $M(x) = g_+(x) + g_-(x)$ which is the sum of two normalized Gaussians of a same second reduced moment μ_2: $g_\pm(x) \sim \exp[-(x \pm a)^2/2\mu_2]$. For such a simple example, $r_4 = 2[1 - 1/(1 + \mu_2/a^2)^2]$ varies in the range 0 to 2. The predicted bimodal behavior for $r_4 < 1$ or unimodal behavior for $r_4 > 1$ can be checked by searching the zeros of the first derivative of $M(x)$. A straightforward calculation shows that the resulting profile is unimodal if $a^2 < \mu_2$ or bimodal if $a^2 > \mu_2$. This simple example shows that the criterion is only indicative. For an even profile $M(x)$, r_4 could also be related to a measure of the flattening out of the curve near the origin. The smaller it is, the flatter the profile.

As an estimation of the linearity of the phase with respect to frequency offset, we used the mean square of the second derivative of the phase with respect to the frequency offset:

$$p_2 \sim \int \left[\frac{d^2S(x)}{dx^2}\right]^2 dx. \qquad [29]$$

It should be close to zero when the phase is nearly linear in frequency offset.

Since the formalism developed above drastically reduces the simulation time, we could perform a brute force simulation of the powder-averaged CES by varying the pulse angles of each pulse of the composite sequence for a given phase cycle. The observed reduced frequency range was set to $x \in [-5.5; 5.5]$, a range large enough to cover at least two secondary lobes around the main one. Moreover, it saves computing time.

To be specific, we chose to fix the preparation pulse angle to $\theta_M = 1$ rad, the pulse angle value which would give the maximum signal after a single-pulse experiment on a powder sample. A smaller angle would increase the bandwidth excitation, but at the expense of the signal-to-noise ratio. Evidently, the first pulse angle should also be varied in a general analysis which seeks for sequences covering a very large spectral excitation. But we considered that fixing the first pulse length to the value which gives the highest signal-to-noise ratio was an interesting starting point.

The choice of the angle step for the pulses of the CPP was dictated by three considerations. First, the angle step must be small enough to cover correctly all the possible cases in a reasonable computing time; second, it is no use considering too small steps since we do not expect abrupt variation of the properties of a sequence with respect to the pulse angles. Moreover, we should also be able to discriminate between the different sequences. Third, the experience showed that, with a power of $\omega_{RF}/2\pi = 13$ kHz, a pulse length step less than 3 μs has little influence on the results. We found that a good compromise is a step of $\Delta\theta \approx 0.25$ rad, the allowed maximum angle value of each pulse being set to 3.5 rad (maximum composite pulse length of $\sim$120 μs). This choice leads to a total of $(14)^3 = 2744$ possibilities for each phase sequence to be calculated. If one needs faster simulations, one can only consider 10 steps ($\Delta\theta \approx 0.35$ rad; 1000 possibilities) instead of 14, thus reducing the calculation time by a factor of $\approx$2.7. We checked that such a resolution is sufficient to select the useful composite echo sequences.

We also limited the pulse phases to the values 0, $\pi/2$, π, and $3\pi/2$. Although this choice was primarily dictated by simplicity and time saving, it is worth noticing that such phase values permit the generation of ideal composite pulse sequences (with no delay between the pulses) when the spectrometer is equipped with an adapted electronics. Since only the relative phases of the different pulses of the composite pulse are relevant, nine different phase cycles must be considered for each set of pulse lengths.

The sequences were selected by using correlation between the first five reduced moments of the excitation profile and the estimator p_2 for phase linearity. At last, a direct visual inspection of the excitation profiles of the sequences selected by the computer was used to select the best one. The HES (θ_M)–τ–$(2\theta_M)$ served as a reference. The reduced moments of the HES are $M_0 \approx 1.6$, $\mu_1 = r_3 = 0$, $\mu_2 \approx 2.02$, and $r_4 \approx 4.66$. The main lobe is almost Gaussian, but the contribution of the two symmetrical secondary lobes appearing in the frequency range considered is not negligible. This explains the discrepancy between the above-quoted reduced moments and the one expected for a pure Gaussian profile.

It is interesting to compare the histograms of the numerical characteristics (the mean M_0, the square root of the second moment $\sqrt{\mu_2}$, the skewness r_3, and the reduced fourth moment r_4) of the excitation profile for different phase cycles of the composite π pulse (Fig. 2). Among the nine possibilities of phase cycles, we remarked that some phase cycles gave the same distribution of the even moments, and thus could be grouped by pairs. This is why only five different sets of data are presented in Fig. 2, the $\{0\ \pi\ 0\}$ phase cycle being a particular case. One should note that the phase behavior with respect to frequency offset may be completely different within a pair of phase cycles for given pulse lengths. Since the distribution of skewness of one sequence of the pair is always the mirror image of the other sequence of the pair, only one is shown.

As indicated by Fig. 2, the $\{0\ \pi\ 0\}$ phase cycle gives the widest mean intensity and second moment distribution. Moreover, whatever the pulse lengths, the excitation profile is symmetric around the excitation frequency. An interesting property of the phase cycle $\{0\ \pi\ 0\}$ is that the phase is almost linear with frequency offset when the first and third pulse of the CPP have an equal length. For a crystal (or for spins $I = \frac{1}{2}$), it is rather easy to prove that if the first and third pulse have the same angle, then the linearity of the phase with respect to the frequency offset is good. Our simulations show that the same conclusion is also valid after powder average, although this result was not evident a priori.

All the other phase cycles seem to give a bad overall phase behavior as a function of frequency offset. Usually, the range of phase linearity is very narrow. The most serious drawback comes from the fact that the phase is usually an even function near the excitation frequency, making the use of a linear phase correction impossible.

As a conclusion, our simulations indicate that the phase cycle $\{0\ \pi\ 0\}$ is the most suitable for giving a phasable spectrum and a large excitation range. The best CES in our opinion is described below.

IV. SIMULATED AND EXPERIMENTAL EXCITATION PROFILES

This section focuses on the properties of the best CES selected from the simulation procedures described in Section III, as compared to the HES (θ_M)–τ–$(2\theta_M)$ and to the SES (θ_M)–τ–(θ_M)–τ'–(θ_M), where $\theta_M = 1$ rad. Such sequences are

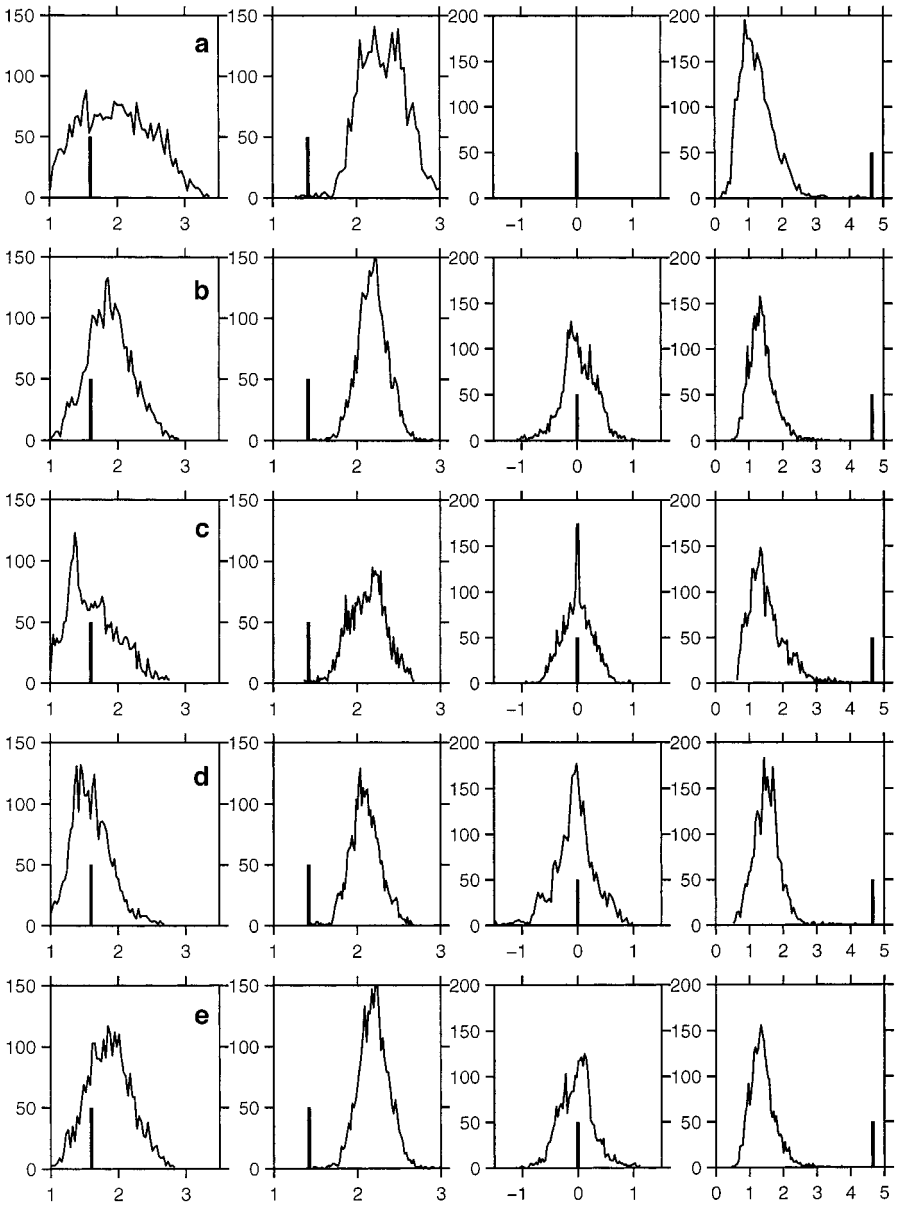

FIG. 2. Histograms of the numerical characteristics of the excitation profile of different CES. The thick vertical bar represents the corresponding value of the HES. The integration range is [−5.5; 5.5]. The columns from left to right present the histograms of M_0, $\sqrt{\mu_2}$, r_3, and r_4. Each line corresponds to a given phase cycle: (a) {0 π 0}; (b) {0 π $\pi/2$} or {0 π $3\pi/2$}; (c) {0 $\pi/2$ 0} or {0 $3\pi/2$ 0}; (d) {0 $\pi/2$ π} or {0 $3\pi/2$ π}; and (e) {0 $\pi/2$ $3\pi/2$} or {0 $3\pi/2$ $\pi/2$}. When two phase cycles are indicated, only one skewness is represented for the sake of clarity since the skewness of one sequence is the mirror image of the other one versus the origin.

optimized for a powder sample. The simulations are then compared to experimental data obtained with chloranil at ambient temperature.

The chloranil powder (Aldrich) was used without purification. It presents two ^{35}Cl lines ($I = \frac{3}{2}$) around 36.855 and 36.785 MHz, depending on temperature, with asymmetry parameter $\eta \approx 0.2$. The linewidth at half-height is a few kilohertz, and is mainly of inhomogeneous nature. The experiments were performed on a Bruker ASX 300 at ambient temperature. The probe full bandwidth at half-height being roughly ~400 kHz, no correction was applied to the data to take into account the apparatus bandwidth. The RF power was $\omega_{RF}/2\pi = 13$ kHz.

All spectra were acquired with quadrature detection and were Fourier transformed after truncation of dead-time points and zero filling. The intensities of the signals were compared by considering a "single-run experiment." In the simulations, it is easy since the right coherence pathways could be implemented directly. For a real experiment, by a "single-run experiment" we mean the accumulation of FIDs with the minimum

phase cycle allowing the chosen coherence pathways to be selected. For instance, all sequences could be implemented with a 16 phase cycling procedure (by steps of $\pi/2$). In order to check the efficiency of the linear phase correction, the experimental data were taken from the height of the peaks that were positive and almost symmetric after the phasing procedure and compared to the modulus of the simulated excitation profile.

We have seen that an ideal composite π pulse is composed of three different pulses placed side by side with no delay between them. However, it was impossible to realize such an ideal sequence with our spectrometer because the phase of each pulse is ill defined when the interpulse delay is set to zero. We found that the minimum time required to set correctly the pulse phase was 3 μs. Therefore, our real "composite π pulse" is composed of three pulses separated by a delay of 3 μs. This delay introduces an inherent dephasing which strongly depends on the frequency offset. For instance, a frequency offset $\Delta\nu \approx$ 20 kHz and a dephasing time of 3 μs give a phase shift of $\sim$0.38 rad, which cannot be neglected. However, such an effect could be easily incorporated into the simulation programs.

We stress that our simulations need only one parameter, the spectrum intensity acquired at resonance with a HES. All the other parameters are known or could be measured. It should also be remembered that the simulations do not take into account the sources of imperfections coming from the spectrometer and the probe.

As already stated, we took as a reference the HES (θ_M)–τ–$(2\theta_M)$ because it is the echo sequence with the best signal-to-noise ratio. The cost of having a "good" signal is evidently a small excitation bandwidth: in reduced frequency units, the full width at half-height is $\Delta x_{1/2} \approx 2.5$. A disadvantage of this sequence is the rather small radius of curvature of the excitation profile near the maximum, giving a rapid signal intensity decrease. As opposed to the HES, the SES (θ_M)–τ–(θ_M)–τ'–(θ_M) excitation bandwidth is twice as large as that of the HES, at the expense of a signal amplitude divided by 2. The simulated excitation profiles and experimental results appear in Fig. 3. The simulated phase is almost linear with frequency offset (not shown), as confirmed by the experimental spectra which could be correctly phased over the whole frequency offset range (Fig. 3b and Fig. 3c).

Among the different CESs with alternating phases [0 π 0], we found that the best spectral excitation was given by a CPP composed of the following pulse angles in radians: $(1)_0$–τ–$(0.35)_0(2.1)_\pi(0.35)_0$ (see Fig. 4). Compared to a classical HES, the excitation bandwidth is enlarged with only a slight decrease in intensity (maximum intensity of 0.5 instead of 0.6: Fig. 4a). Thus, the signal-to-noise ratio remains good. Moreover, the phase shift has almost the same behavior as the HES, allowing a linear correction of the spectrum (Fig. 4b). Another interesting feature of the ideal CPP is that the excitation amplitude is almost constant within $\Delta x = \pm 1$ around the excitation frequency. In fact, the central lobe has two maxima, which fortunately almost merge into a single broad peak. Two secondary lobes of nonnegligible intensity are also visible in the frequency range of study.

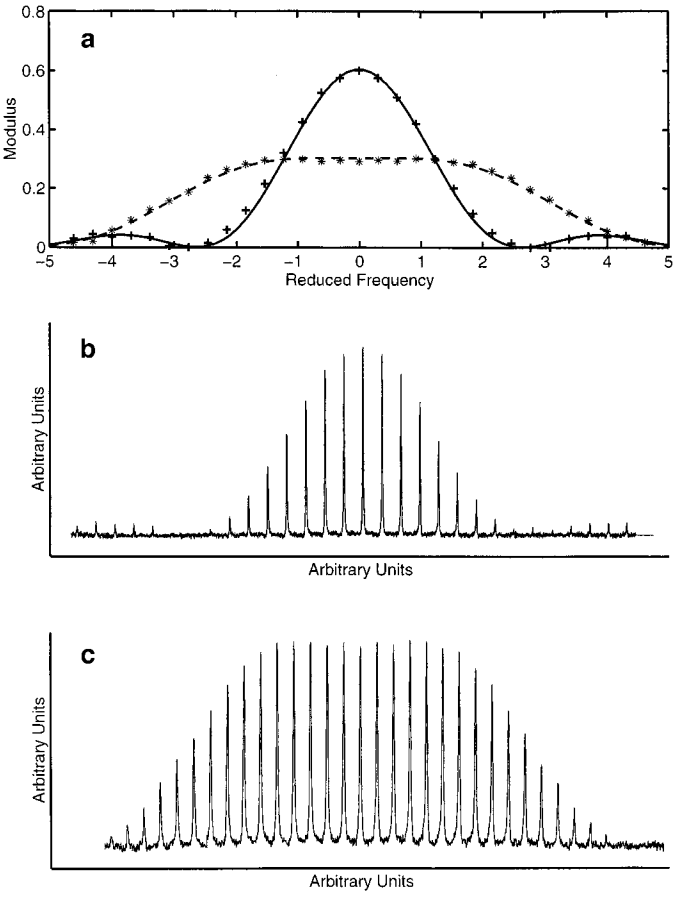

FIG. 3. Simulated and experimental excitation profiles of the Hahn (HES) and stimulated (SES) echo sequences. (a) Experimental amplitudes: (*) HES and (+) SES (reduced frequency offset $x = \omega/\omega_{RF}$) and $\omega_{RF}/2\pi = 13$ kHz); simulated excitation profiles: solid and dashed lines. (b) and (c) Real part of the phased spectra for respectively the HES (b) and the SES (c). The frequency step between two spikes is 4 kHz. Note that the experimental spectra are not lined up with (a).

Concerning the nonideal CPP, the main effect of the interpulse delay is to make the two maxima of the modulus more pronounced, and to slightly reduce the excitation bandwidth. This modulation of the excitation profile may be a major drawback in the study of spectra patterns. We found that this modulation could be partly reduced by increasing the middle pulse angle (with our experimental conditions, we used a 2.2-rad pulse instead of 2.1 rad), at the expense of another small reduction of the excitation bandwidth. Note that the phase behavior is almost not affected by the interpulse delay, whereas the secondary lobe's intensity increases.

The experimental data (Fig. 4c) and the simulations are compared in Fig. 4a. The agreement is correct if the interpulse delay is taken into account in the simulations, although the

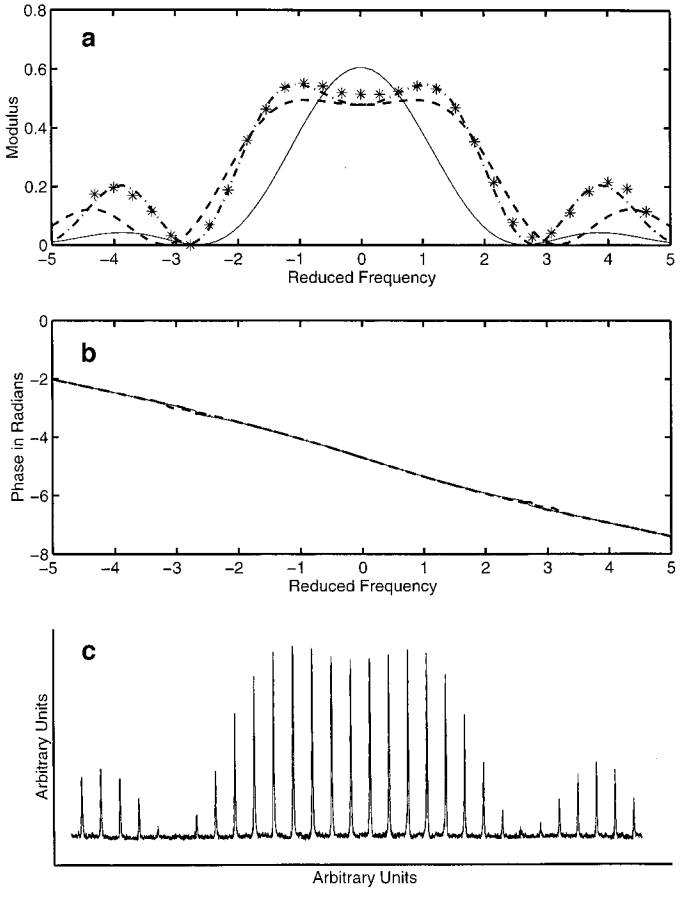

FIG. 4. Simulated and experimental excitation profiles of the optimized three-pulse composite echo sequence: $(1)_0$–τ–$(0.35)_0(2.1)_\pi(0.35)_0$. (a) (*) Experimental data (reduced frequency offset $x = \omega/\omega_{RF}$) and $\omega_{RF}/2\pi = 13$ kHz). The lines represent different simulations: dashed line, sequence with an ideal composite π pulse; dash-dot line, sequence with a "real" composite π pulse where the interpulse delay is 3 μs; and solid line, HES. (b) Phase (in radians) of the different sequences. (c) Phased experimental spectra. Note that this spectrum is not aligned with (a). The frequency step between two spikes is 4 kHz.

modulation of the excitation profile near the excitation frequency is not perfectly reproduced. However, we see that the modulation is less pronounced in the experimental data than predicted by the theory.

In view of these results, the composite echo sequence $(1)_0$–τ–$(0.35)_0(2.1)_\pi(0.35)_0$ may be a good alternative to a HES if one needs a good signal-to-noise ratio.

Besides the problem of having a large excitation bandwidth which is as flat as possible and whose phase shift is linear in frequency, a crucial problem in pure NQR is to find the resonance frequency of a given nuclei. In that case, the phase is not a problem since the modulus contains enough information to find the signal. Therefore, one looks for a sequence giving a good signal-to-noise ratio with a large excitation bandwidth. Some sequences are proposed in Fig. 5.

V. SINGLE-CRYSTAL VERSUS POWDER-AVERAGED EXCITATION BANDWIDTH

In the previous sections, we optimized the excitation bandwidth of the sequences for a powder sample. However, it is also interesting to evaluate the performance of these sequences on a single crystal.

For a single crystal, the signal is a function of the value of the angular factor λ imposed by the asymmetry parameter and the relative orientation of the coil with respect to the PAS. The range of the values of λ depends on the asymmetry parameter, but it can be easily shown that $0 \leq \lambda \leq 1$. For $\lambda = 0$, the signal is zero, so we performed the single-crystal simulations starting at $\lambda = 0.1$.

In order to draw a comparison between the different sequences, we chose to restrict the study to the main lobe of the excitation profile, in contrast to the approach of the previous

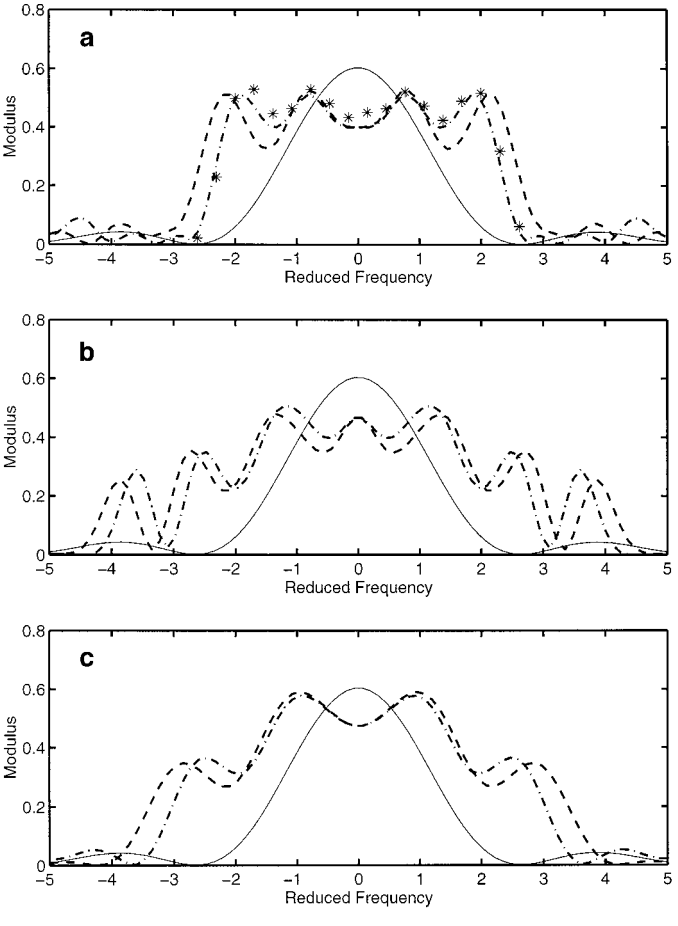

FIG. 5. Broadband excitation profiles of different CES. The thin line is the excitation profile of the HES. Dashed line, no delay between pulses; dash-dot line, delay of 3 μs. (a) $(1)_0$–τ–$(3.14)_0(1.4)_\pi(3.5)_0$, the phase is almost constant in the range $[-2.5\ 2.5]$; (*) experimental data (reduced frequency offset $x = \omega/\omega_{RF}$) and $\omega_{RF}/2\pi = 13$ kHz); (b) $(1)_0$–τ–$(2.44)_0(3.5)_\pi(2.44)_0$, the phase is almost linear in frequency offset; (c) $(1)_0$–τ–$(2.44)_0(1.4)_\pi(0.35)_0$, the phase is ill behaved.

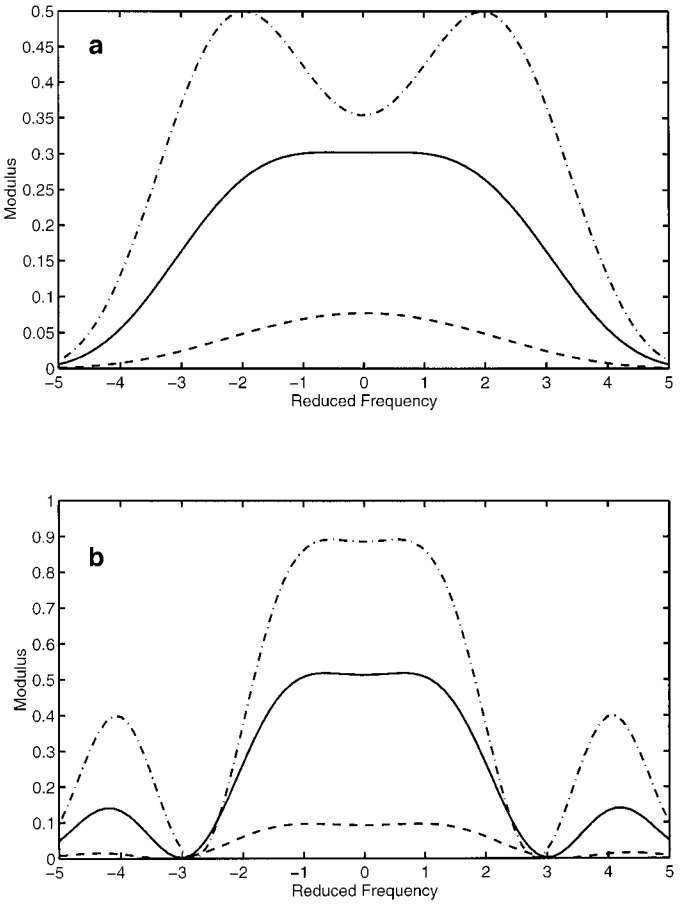

FIG. 6. Comparison of the modulus of the excitation profiles of a single crystal and a powder. (a) SES; (b) CES $(1)_0$–τ–$(0.35)_0(2.1)_\pi(0.35)_0$. Solid line, powder average with $\eta = 0.5$; dashed line, $\lambda = 0.4$; dash-dot line, $\lambda = 1$. The composite pulse was supposed ideal.

sections where we used a common frequency range that could also include secondary lobes. The moments of the excitation profile were calculated on the following range of reduced frequency: $[-3; 3]$ for the CES $(1)_0$–τ–$(0.35)_0(2.1)_\pi(0.35)_0$, $[-2.5; 2.5]$ for the HES, and $[-5; 5]$ for the SES. Since the excitation profile is an even function of the frequency, the standard deviation and the reduced fourth moment are sufficient to give a characterization of the excitation bandwidth. The powder average uses $\eta = 0.5$, because the asymmetry parameter has a negligible effect on the values of the moments.

Figure 6 compares the variation of the modulus of the excitation profile as a function of frequency offset for two different values of λ with the powder-averaged signal. Evidently, the signal amplitude is a fast decreasing function of λ. Although not shown, it is worth noting that the phase is always more linear with respect to the frequency offset for a powder than for a single crystal. The discrepancy between a single crystal and a powder-averaged signal is the strongest for the SES: the excitation profile becomes bimodal at high values of λ.

These trends are the best quantified by the variation of the standard deviation and the reduced fourth moment of the main lobe for different values of λ for a single crystal, as presented in Fig. 7. The stimulated echo sequence SES strongly depends on the λ value, whereas the HES and CES weakly vary with λ. Moreover, the deviation from the powder-averaged value is less than $\approx$16%. Therefore, the SES is only efficient on a powder when one is interested in a large and flat excitation profile around the irradiation frequency. In contrast to the SES, the optimized CES seems relatively insensitive to the value of λ, and is thus also expected to give good results on a single crystal.

VI. RECONSTRUCTING A LARGE SPECTRUM WITH A CES

The spin echo mapping method developed by Bussandri and Zuriaga (*10*) for reconstructing large spectra can also be implemented with a CES. The principle of the method is to use

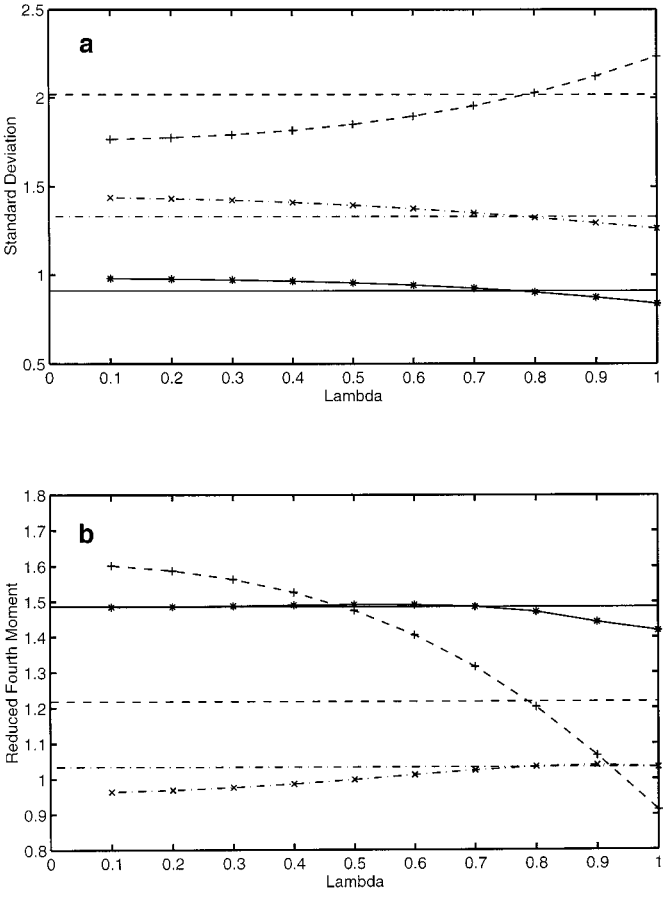

FIG. 7. Standard deviation and reduced fourth moment of the main lobe of the excitation profile of the HES, SES, and CES for different values of the angular factor λ. The horizontal lines result from a powder average with $\eta = 0.5$. (a) Standard deviation. (b) Reduced fourth moment. Solid line and *, HES; dashed line and +, SES; dash-dot line and $\times$, CES $(1)_0$–τ–$(0.35)_0(2.1)_\pi(0.35)_0$. The composite pulse was supposed ideal.

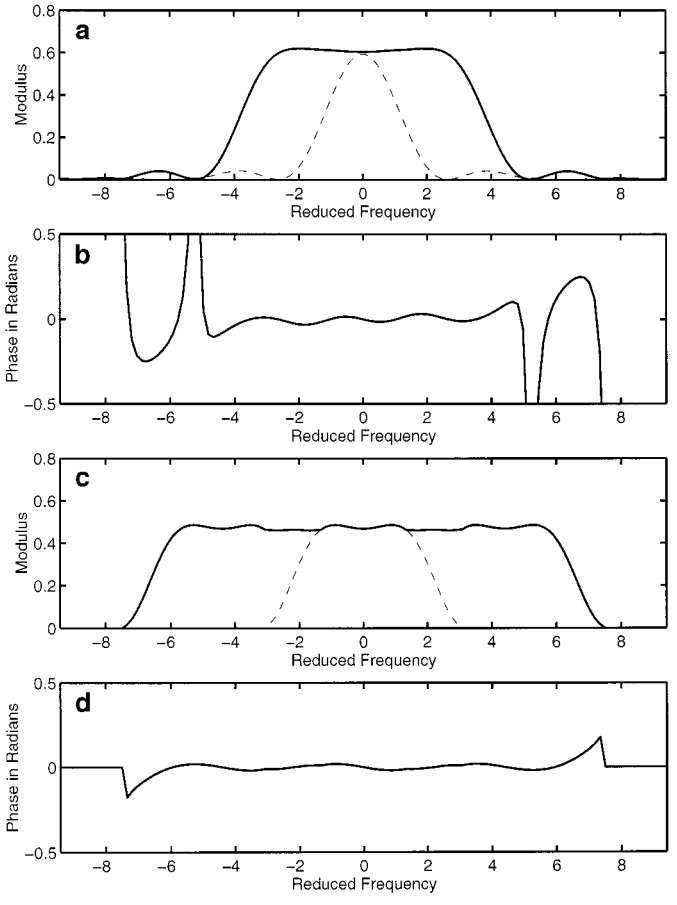

FIG. 8. Spectrum reconstruction by adding different spectra acquired at different irradiation frequencies. (a) and (b) HES, irradiation frequencies x_{irr} at 0 and ± 2.5; (c) and (d) CES $(1)_0$–τ–$(0.35)_0(2.1)_\pi(0.35)_0$, irradiation frequencies x_{irr} at 0 and ± 4.4. In (a) and (c), the dashed line is the excitation profile at irradiation frequency 0. The spectra were phased independently before summation. For the CES, the data were truncated before summation by keeping only the principal lobe in the reduced frequency range $[x_{irr} - 3\ x_{irr} + 3]$.

the addition of spectra acquired at different irradiation frequencies, with a constant frequency step chosen small enough in order to have a flat excitation profile.

Figure 8 illustrates the spin echo mapping method implemented with the HES and the CES echo sequences. Three irradiation frequencies x_{irr} were used, but the method can be evidently generalized to more irradiation frequencies. Each spectrum was phased in the same way, and truncated to keep the main lobe around the irradiation frequency by replacing the unwanted data points by zero points. This truncation is always necessary to keep a good signal-to-noise ratio. Concerning the spectra acquired with the CES, the truncation also has the role of suppressing the secondary lobes having nonnegligible amplitude. Otherwise, the resulting profile would not be flat. The main lobe of the CES lies in the reduced frequency interval $[x_{irr} - 3\ x_{irr} + 3]$.

Making several attempts, we found that the best irradiation frequency step is $\Delta x = 2.5$ for the HES whereas it is $\Delta x = 4.4$ for the optimized CES. As shown in Figs. 8a and 8c, the excitation profile resulting from the addition of different CES spectra is not as flat as the one obtained with the HES, but the departure from a constant profile remains small and is sufficient for reconstructing large spectra. Note that the phase is almost constant with respect to the frequency offset in the main excitation range.

Thus, the use of the CES to reconstruct large spectra reduces the experimental time by a factor of ≈ 1.7 if compared to the HES, and gives almost the same signal-to-noise ratio.

VII. CONCLUSION

This article focused on the conceiving of an echo sequence composed of a single preparation pulse and a composite transfer pulse made of three pulses, which would give a large and flat excitation profile around the excitation frequency, as well as a good phase linearity with respect to the frequency offset. For the first time, an echo sequence optimized to compensate off-resonance effects as well as the intrinsic pulse angle distribution in spin $\frac{3}{2}$ pure NQR of powder samples is presented.

We emphasized the fact that, in NQR of a powder sample, the echo sequence must be optimized *as a whole* because both the excitation and the reception are angular dependent. The calculations rely on the framework of the Cayley–Klein matrices to handle space rotations, which we adapted to calculate the time evolution of the density matrix in the rotating frame. Combined with a fast powder-averaging procedure described elsewhere (*11*), it permitted a numerical approach to optimizing the excitation profile.

The sequences were distinguished by the use of the first five reduced moments of the excitation profile as well as an estimator of the phase linearity. Simulations over typically more than 20,000 sequences lead to the result that the most efficient echo sequence, according to the above criteria which are somehow subjective, is the following: $(1)_0$–τ–$(0.35)_0(2.1)_\pi(0.35)_0$. The performance of this sequence was compared to that of the classical two-pulse Hahn echo sequence and the three-pulse stimulated echo sequence. The loss of signal-to-noise ratio if compared to the Hahn echo is small, whereas the excitation bandwidth is multiplied by roughly 1.7. Experimental data obtained on chloranil confirmed the simulations, which also take into account the small delay imposed by the spectrometer electronics between the pulses. Although optimized for a powder sample, we showed that this sequence should give good results with a monocrystal, in contrast to the stimulated echo sequence.

Since the reconstruction of large spectra with the proposed CES is faster by a factor of 1.7 if compared to the use of a conventional Hahn echo, we hope such a possibility will be useful to experimenters working on the physics of systems presenting large distributions of quadrupolar interactions (glasses, incommensurate systems, high-temperature supercon-

ductors, alloys, etc.). The simulation and optimization procedures can also be applied to more complicated sequences.

APPENDIX

The probability density of the angular factor λ is

$$g(\lambda) = \frac{2u^2}{|v|}\,\lambda D\left(\frac{(u\lambda)^2 - w}{v}, f\right), \qquad [A1]$$

where

$$u = 2\sqrt{3 + \eta^2}; \quad v = 3(\eta - 3)(\eta + 1);$$
$$w = (3 + \eta)^2; \quad f = \frac{-12\eta}{v}, \qquad [A2]$$

and the function $D(y, f)$ is defined by

$$D(y, f) = \begin{cases} y < f, & \dfrac{1}{\pi\sqrt{f(1-y)}}\,K\left(\dfrac{y(1-f)}{(1-y)f}\right) \\ y > f, & \dfrac{1}{\pi\sqrt{y(1-f)}}\,K\left(\dfrac{f(1-y)}{(1-f)y}\right) \end{cases}, \qquad [A3]$$

where K is the complete elliptic integral of the first kind

$$K(m) = \int_0^{\pi/2} \frac{dx}{\sqrt{1 - m\,\sin^2(x)}}.$$

ACKNOWLEDGMENTS

The author is particularly indebted to J. Gallier and M. Buron-Le Cointe for fruitful discussions.

REFERENCES

1. R. Freeman, S. P. Kempsell, and M. H. Levitt, Radiofrequency pulse sequences which compensate their own imperfections, *J. Magn. Reson.* **38,** 453–479 (1980).
2. A. J. Shaka and A. Pines, Symmetric phase-alternating composite pulses, *J. Magn. Reson.* **71,** 495–503 (1987).
3. M. H. Levitt and R. R. Ernst, Composite pulses by a recursive expansion procedure, *J. Magn. Reson.* **55,** 247–254 (1983).
4. R. Tycko, Broadband population inversion, *Phys. Rev. Lett.* **51,** 775–777 (1983).
5. W. S. Warren and A. H. Zewail, Multiple phase-coherent laser pulses in optical spectroscopy. I. The technique and experimental applications, *J. Chem. Phys.* **78,** 2279–2297 (1983).
6. A. Ramamoorthy, N. Chandrakumar, A. K. Dubey, and P. T. Narasimhan, Analysis of the performance of NQR composite pulses, *J. Magn. Reson. A* **102,** 274–286 (1993).
7. A. Ramamoorthy and P. T. Narasimhan, Broadband excitation sequences for NQR spectroscopy, *Mol. Phys.* **73,** 207–219 (1991).
8. A. Ramamoorthy, Phase-alternated composite pulses for zero-field NMR spectroscopy of spin 1 systems, *Mol. Phys.* **93,** 757–766 (1998).
9. S. Z. Ageev, D. J. Isbister, and B. C. Sanctuary, Composite pulses in nuclear quadrupole resonance, *Mol. Phys.* **83,** 193–210 (1994).
10. A. P. Bussandri and M. J. Zuriaga, Spin-echo mapping spectroscopy applied to NQR, *J. Magn. Reson.* **131,** 224–231 (1998).
11. C. Odin, Calculations of multipulse sequence in NQR of spins $\frac{3}{2}$, *J. Magn. Reson.,* **141,** 239–255 (1999).
12. J. C. Pratt, P. Raghunathan, and C. A. McDowell, Transient response of a quadrupolar spin system in zero applied field, *J. Magn. Reson.* **20,** 313–327 (1975).
13. J. C. Pratt, Nuclear quadrupole resonance in the interaction representation, *Mol. Phys.* **34,** 539–555 (1977).
14. S. Su and R. L. Armstrong, Bromine resonance in PrBr3 as an example of mixed spin echoes in pure nuclear quadrupole resonance, *J. Magn. Reson. A* **101,** 265–276 (1993).
15. M. Goldman, Spin-$\frac{1}{2}$ description of spins $\frac{3}{2}$, *Adv. Magn. Reson.* **14,** 59–74 (1990).
16. C. P. Slichter, "Principles of Magnetic Resonance," 3rd ed. Springer-Verlag, Berlin/New York (1990).
17. K. Schmidt-Rohr and H. W. Spiess, "Multidimensional Solid-State NMR and Polymers," Academic Press, San Diego (1994).
18. R. R. Ernst, G. Bodenhausen, and A. Wokaun, "Principles of Nuclear Magnetic Resonance in One and Two Dimensions," Clarendon Press, Oxford (1994).
19. D. A. Varshalovich, A. N. Moskalev, and V. K. Khersonskii, "Quantum Theory of Angular Momentum," World Scientific, Singapore (1988).
20. S. Sternberg, "Group Theory and Physics," pp. 4, 21, Cambridge Univ. Press, Cambridge, UK (1994).
21. M. Tinkham, "Group Theory and Quantum Mechanics," pp. 103–106, McGraw–Hill, New York (1964).
22. N. Ja. Vilenkin, "Fonctions Spéciales et Théorie de la Représentation des Groupes," p. 91, Dunod, Paris (1969). [Translated from Russian]